Available online at www.sciencedirect.com
ScienceDirect
Mathematical Biosciences 212 (2008) 22–53
Mathematical Biosciences
www.elsevier.com/locate/mbs

A computational model of the human thyroid

Mike Degon [a,b], Stuart R. Chipkin [c,d], C.V. Hollot [e], R. Thomas Zoeller [f], Yossi Chait [b,*]

[a] USUHS School of Medicine, Bethesda, MD 20814, USA
[b] Mechanical & Industrial Engineering Department, UMass, Amherst, MA 01003, USA (formerly)
[c] Valley Medical Group, Florence, MA 01060, USA
[d] Department of Kinesiology, UMass, Amherst, MA 01003, USA
[e] Electrical & Computer Engineering Department, UMass, Amherst, MA 01003, USA
[f] Biology Department, UMass, Amherst, MA 01003, USA

Received 3 August 2006; received in revised form 30 September 2007; accepted 26 October 2007
Available online 6 November 2007

Abstract

The thyroid, the largest gland in the endocrine system, secretes hormones that help promote bodily growth and development. This gland regulates hormonal secretion rate in spite of changes in dietary iodine which is a key ingredient in the hormone's biosynthesis. The thyroid relies on several feedback mechanisms for this regulation, and in this paper we use recent molecular-level and clinical observations to engineer a computational thyroid model. We use simulation and analysis to show that this models captures known aspects of thyroid physiology. We identify features in the model that are responsible for hormonal regulation, and use the model to identify and evaluate competing hypotheses associated with Wolff–Chaikoff escape.

Keywords: Thyroid; Systems biology; Pharmacodynamic model

* Corresponding author. Tel.: +1 413 545 0134; fax: +1 413 545 1027.
E-mail address: chait@ecs.umass.edu (Y. Chait).

0025-5564/$ - see front matter © 2008 Published by Elsevier Inc.
doi:10.1016/j.mbs.2007.10.009

Nomenclature

AIT Apical I^- transporter
DIT/MIT Mono-iodinated/Di-iodinated Tyrosyl (μg)
H_2O_2 Hydrogen Peroxide (ng)
I_{in} Dietary iodine intake (μg)
I_S, I_F, I_C Inorganic iodide in extracellular fluid, follicle cells, colloid (μg)
I_H^* Organic iodide bound to thyroid hormone precursors (μg)
I_H Organic iodide bound to thyroid hormone (μg)
I_{MD}^* Organic iodide bound to iodotyrosyl precursors (μg)
I_{MD} Organic iodide bound to MIT/DIT (μg)
I_{T_3}/I_{T_4} Organic iodide content in T_3/T_4 (μg)
I_{Tg} Organic iodide content of thyroglobulin in the colloid (μg)
I_{Vac} Organic iodide content of thyroglobulin in vacuoles (μg)
NIS Na^+/I^- Symporter (pmol)
rT_3 3,3′,5′-Triiodothyronine
$\mathcal{S}_y^x$ Stimulatory gain of x on y
SSF Secondary signaling factor
T_3 3,5,3′-Triiodothyronine
T_4 Tetraiodothyronine or levothyroxine
TSH Thyroid Stimulating Hormone (mU)
TSH-R TSH Receptor
Tg Thyroglobulin (mg)
TPO Thyroid Peroxidase (μg)
V_{ac} Vacuoles (mL)
A_x/Vol_x Surface area/volume of x (m^2/m^3)
α_x, K_x Constants
K_y^x/V_y^x Michaelis/velocity constants
$[x]$ Concentration of x

1. Introduction

The thyroid is the largest gland in the endocrine system. It secretes hormones that help promote bodily growth and development. Using molecular-based tools, researchers have identified signalling pathways within the thyroid that help explain some of its disorders. However, these discoveries have had limited impact on clinical practice including the recommended iodine dosage following a nuclear accident [1], and risk assessment for environmental contaminants such as perchlorate [2,3]. While clinical studies are ultimate arbiters of a protocol's success, they may be of less value in protocol design. Clinical studies require careful planning, evolve on long time scales, are constrained by the capabilities of instrumentation, and are of limited use in studying behavior

under toxic conditions. A complementary approach – the focus of this paper – is to develop a high-fidelity computational model that can be used to predict thyroid function under different physiological conditions. Using this model, targeted computational studies could offer new understanding and suggest hypotheses to produce better-focused clinical studies, which may eventually lead to improved protocols.

The Hypothalamus–Pituitary–Thyroid (HPT) axis in Fig. 1 is a feedback system that uses hormones as signals to regulate the synthesis and release of thyroid hormones T_3 and T_4. These hormones promote bodily growth and help regulate metabolism and energy usage. In response to hormonal signals, the hypothalamus secretes thyrotropin-releasing hormone (TRH) which binds to receptors on the thyroid gland, stimulating synthesis and secretion of thyroid hormones that affect virtually all body cells.

Computational models of the thyroid are based on iodide metabolism steps. Early research [4] used a 3-compartment model to represent the pool dynamics for blood hormone, blood iodine, and intrathyroidal iodine. However, such models could not accurately predict non-euthyroid function; e.g., see [5]. In [6], research on pertechnetate uptake used a 3-compartment model of the thyroid which included iodine pools in the follicular cells and colloid. In [5], the authors developed an 18-compartment model of human iodine metabolism, but only two compartments were devoted to describe intrathyroidal iodine dynamics. A multi-compartmental model including three intrathyroidal pools was developed to quantify the effects of perchlorate on thyroid status and circulating thyroid hormones [7]. In [9,10], researchers considered whole-body thyroid models and used feedback control concepts to prescribe hormone-replacement therapies and to understand the regulation of hormone pool sizes. A dynamical model of the HPT-axis was developed in [8] by fitting model parameters to match clinical data. However, the ability of this model to predict thyroid behavior for different physiological conditions was not explored. Recently, [11] developed a more refined model for the pituitary–thyroid axis and thyroid-hormone metabolism

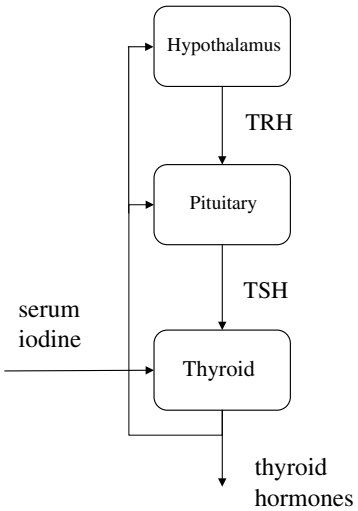

Fig. 1. The hypothalamus–pituitary–thyroid (HPT) axis. In response to hormonal signals, the hypothalamus secretes TRH which stimulates the pituitary to secrete TSH. TSH then acts as a set-point command for the thyroid to synthesize its hormones, whose main synthesis component is serum iodine.

in order to study possible feedback structures that may play a role in the generation of TSH pulses in the human pituitary. However, this analysis relies on a static intrathyroidal model.

The goal of our research is to incorporate recent discoveries of intrathyroidal cell biology to refine computational models of intrathyroidal iodide[1] metabolism. We treat the thyroid as a dynamical system having two exogenous input variables, TSH and plasma iodide levels, and one output, thyroid hormone secretion rate. Specifically, our model consists of 6 iodide pools and 5 protein pools (such as NIS and TPO). As such, it can be combined with whole-body iodine-metabolism models. DiStefano and colleagues have shown early on using qualitative reasoning [12], and very recently in a quantitative study of $L-T_4$ bioequivalence for hormone replacement therapy ([13]), that the TSH to thyroid secretion rate relationship is a simple gain. Our model explicitly includes iodine intake as an input variable and via analysis and simulations we show that the properties of the dynamics of thyroid secretion rate response to TSH are very different from that to iodine intake.

This paper is organized in several major sections. In Section 2 we lay out the qualitative relationships among the thyroid model's inputs, output, and internal thyroid pools. In Section 3 we present a set of non-linear differential equations comprising this model. Section 4 examines the thyroid feedback mechanisms via analysis and simulations, and illustrates how the model can be used for hypothesis testing. Section 5 discusses the implications of the model and possible future applications. The appendices provide details of the derivation of the thyroid model, numerical values for the model's parameters, and our rudimentary model of the whole-body iodine metabolism.

2. System model of the thyroid

In developing the thyroid model we first model a single follicle and use that to produce an integrated model based on aggregation of the single follicle. Such an assumption is a well accepted practice in engineering (e.g., [14,15]) where the complexity related to heterogeneity can be simplified in input–output models such as ours.

As a dynamic system, the thyroid consists of three parts: primary thyroid states (the iodide pools and related bio-processes), TSH stimulation pathways, and inhibitory processes. We discuss each of these three features below in detail. The basis for our discussions can be found in numerous sources focused on endocrinology; for example see [16]. Further details on the development of our model can be found in earlier versions of this model [17,18].

2.1. Iodide pools and biochemical processes

The functional unit of the thyroid is the follicle comprised of follicular cells which surround a protein matrix or colloid. The basolateral and apical membranes form the transport boundaries

[1] The terms iodine and iodide are generally not interchangeable. Iodine is a generic term that includes iodine in all its forms, inorganic or organic. Iodide refers specifically to the inorganic anion I^-. In this paper, we use both organic and inorganic iodide for the various intrathyroidal pools; we use iodide to generically refer to the various forms in the plasma as a single pool that is available for uptake and urine clearance.

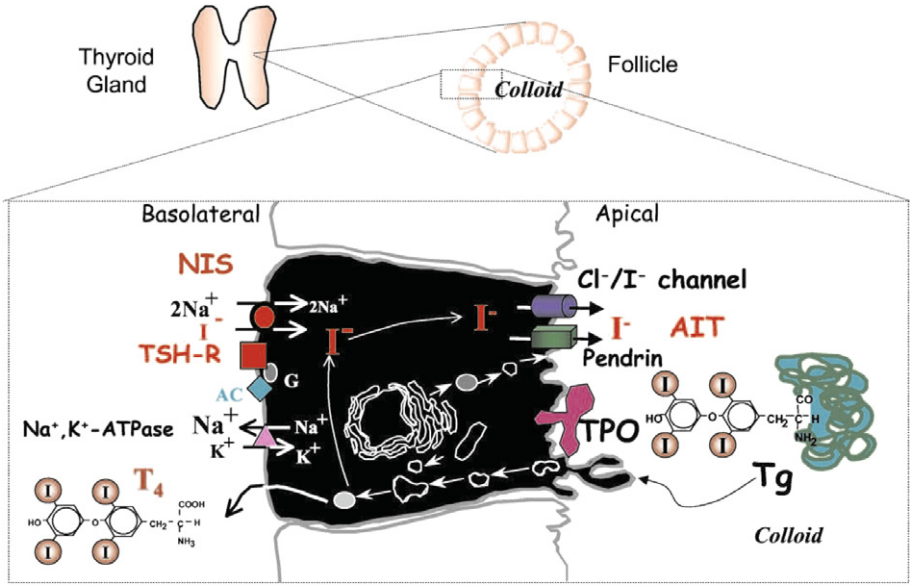

Fig. 2. Schematic of the hormone synthesis pathways within the thyroid follicle. The basolateral and apical membranes form the transport boundaries between the blood stream and colloid, respectively [19]. (Copyright 2003, The Endocrine Society).

between the blood stream and colloid. The iodide path shown in Fig. 2 is as follows. Sodium/iodide Na^+/I^- transporter (NIS) channels act as pumps to transport plasma iodide I_S across the basolateral membrane into the follicular inorganic iodide pool I_F. Next, the process of iodide organification takes place after the protein Pendrin/AIT moves iodide across the apical membrane into the colloid iodide pool I_C, thereby allowing the enzyme Thyroid Peroxidase (TPO) to combine iodide with tyrosine residues attached to Thyroglobulin (Tg). In a second process catalyzed by TPO, the iodinated tyrosine-residues within the Tg molecule are coupled to form the mature molecule containing the precursors to Triiodothyronine (T_3) and Tetraiodothyronine (T_4). This iodinated Tg pool I_{T_g} undergoes endocytosis (bringing colloidal material into the follicular cell) and proteolysis (cleaving the thyroglobulin molecule to release thyroid hormones T_3 and T_4). Some inorganic iodide leaks back down its concentration gradient into the plasma.

2.2. TSH stimulatory pathways

The iodide transport-processes shown in Fig. 3 are stimulated or inhibited by various control signals within the thyroid. The transport promotor that stimulates nearly every aspect of hormone synthesis is TSH which is generated by the pituitary. TSH accomplishes its task through two secondary messenger pathways, the adenyl cyclase and phospholipase C pathways [20]. For purposes of our model, we combine these pathways into a single state, the Secondary Signaling Factor (SSF). TSH stimulates the production of NIS [21], TPO, Tg, and H_2O_2 [22]. TSH also promotes endocytosis, the proteolysis of Tg [23], and triggers follicular cells to increase their volume [16]. TSH has a number of other effects within and outside the thyroid – including increased vascular flow [24] – but these compensate for the increased energy and nutrients required in hormone

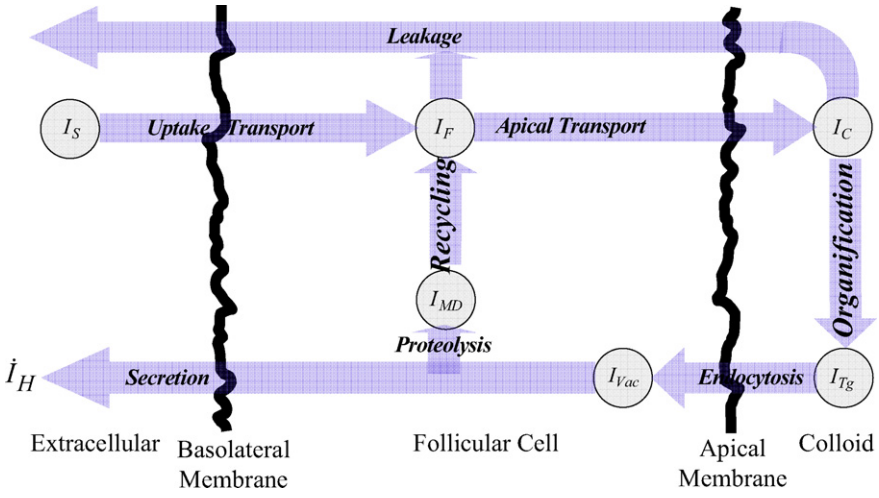

Fig. 3. Schematic representation of thyroid iodide fluxes (thick arrows represent transport processes and circles represent biochemical pools).

synthesis and are excluded from our model. In addition, we neglect the effects of TSH on blood flow across the basolateral membrane that can increase iodine uptake. Fig. 4 incorporates these stimulatory effects of TSH into the thyroid schematic.

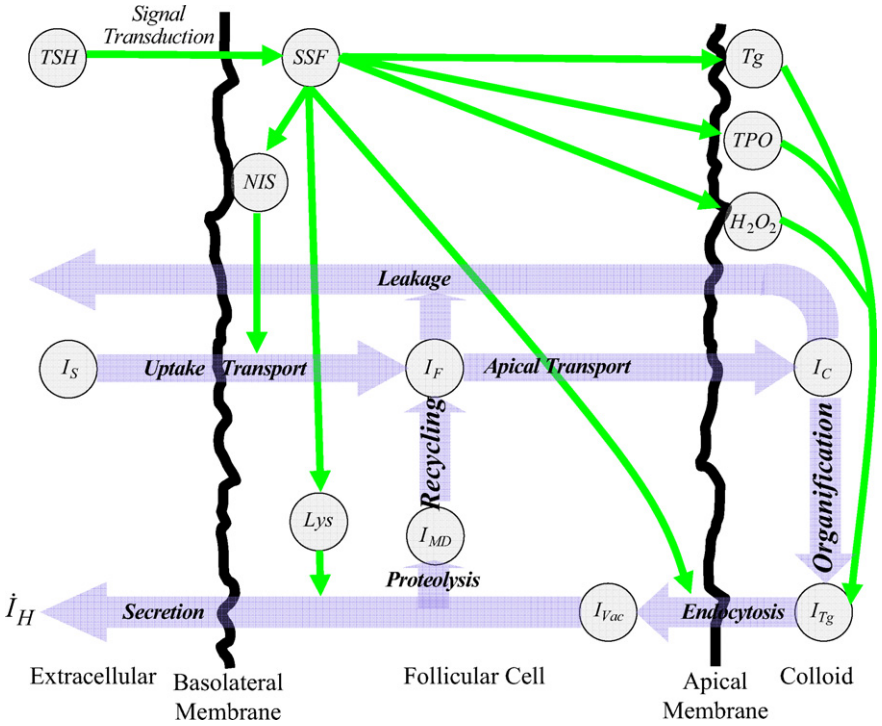

Fig. 4. Schematic representation of thyroid iodide fluxes with TSH stimulation pathways (thick arrows represent transport processes, solid lines represent stimulation, and circles represent biochemical pools).

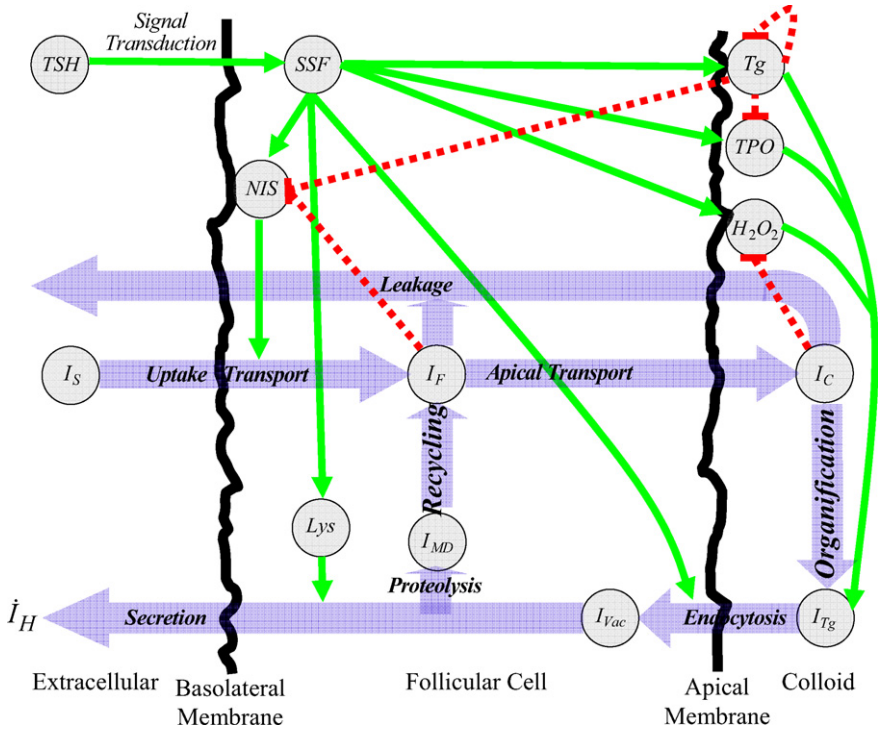

Fig. 5. Schematic representation of thyroid iodide fluxes with TSH stimulation pathways and key inhibition pathways (thick arrows represent transport processes, solid lines represent stimulation, dashed lines represent inhibition, and circles represent biochemical pools).

2.3. Inhibitory pathways

It is well known that the thyroid is capable of dealing with fluctuations in plasma iodide levels. For example, elevated blood iodide levels acutely inhibit iodide organification. This phenomenon is classically referred to as the Wolff–Chaikoff block [22] which is thought to come about from the inhibitory action of intracellular iodide on the organification process [22].[2] Intracellular iodide levels appears to be involved in helping the thyroid escape from this block by inhibiting transcription of NIS [25] and promoting NIS protein turnover [26], thereby reducing the thyroid's ability to transport plasma iodide into the follicular iodide pool. Also, it has been recently suggested that thyroglobulin inhibits itself and transcription of NIS, TPO, and TSH-R [27]. Adding these inhibitory pathways completes our qualitative model as shown in Fig. 5.

[2] Specifically, intracellular iodide levels inhibit the synthesis of Hydrogen Peroxide, H_2O_2, a key component in iodide organification.

3. The thyroid model

In this section we present the non-linear differential equations that comprise our thyroid model as depicted in Fig. 5. Details of the derivations can be found in Appendix A, with the associated parameters given in Table B.1. The model is logically divided into four groups of equations describing the dynamics of the: iodide pools, key biochemicals taking part in the biosynthesis of thyroid hormones, cell volume, and the stimulatory effects of TSH via secondary signaling pathways.[3]

3.1. Iodide pools

The equations in this group describe the dynamics of the inorganic and organic iodide pools: (1) inorganic iodide content within the plasma I_S, follicular cells I_F, and colloid I_C and (2) organic iodide content in thyroglobulin I_{Tg}, secreted thyroid hormones I_H, and iodotyrosol precursors I_{MD}.

$$\begin{aligned}
\frac{\mathrm{d}}{\mathrm{d}t}I_F &= \frac{K_{turnover}^{NIS}[NIS][I_S]}{K_m^{NIS}+[I_S]}A_{basal} + \frac{V_{rec}^{I_{MD}}[I_{MD}]}{K_{rec}^{I_{MD}}+[I_{MD}]}Vol_{follicle} - \alpha_{dif}^{I_F}[I_F]^2 A_{basal} \\
&\quad - \mathcal{S}_{apical}^{SSF}\frac{\alpha_{apical}^{I_C}}{K_{apical}^{I_C}+[I_C]^3}\left(\frac{V_1^{apical}[I_F]}{K_{m1}^{apical}+[I_F]}+\frac{V_2^{apical}[I_F]}{K_{m2}^{apical}+[I_F]}\right)A_{apical} \\
\frac{\mathrm{d}}{\mathrm{d}t}I_C &= \mathcal{S}_{apical}^{SSF}\frac{\alpha_{apical}^{I_C}}{K_{apical}^{I_C}+[I_C]^3}\left(\frac{V_1^{apical}[I_F]}{K_{m1}^{apical}+[I_F]}+\frac{V_2^{apical}[I_F]}{K_{m2}^{apical}+[I_F]}\right)A_{apical} \\
&\quad - \mathcal{S}_{apical}^{SSF}\alpha_{endo}\frac{A_{apical}}{A_{apical,nom}}[I_C] \\
&\quad - \tau_{turnover}^{TPO}[TPO]\frac{V_{org}^{H_2O_2}[H_2O_2]}{K_{org}^{H_2O_2}+[H_2O_2]}\frac{V_{org}^{I_C}[I_C]}{K_{org}^{I_C}+[I_C]}\frac{V_{org}^{Tg_{eff}}[Tg_{eff}]}{K_{org}^{Tg_{eff}}+[Tg_{eff}]} \\
\frac{\mathrm{d}}{\mathrm{d}t}I_{Tg} &= \tau_{turnover}^{TPO}[TPO]\frac{V_{org}^{H_2O_2}[H_2O_2]}{K_{org}^{H_2O_2}+[H_2O_2]}\frac{V_{org}^{I_C}[I_C]}{K_{org}^{I_C}+[I_C]}\frac{V_{org}^{Tg_{eff}[Tg_{eff}]}}{K_{org}^{Tg_{eff}}+[Tg_{eff}]} \\
&\quad - \mathcal{S}_{apical}^{SSF}\alpha_{endo}\frac{A_{apical}}{A_{apical,nom}}[I_{Tg}] \\
\frac{\mathrm{d}}{\mathrm{d}t}I_H &= \mathcal{S}_{proteo}^{Lys}\frac{V_{proteo}^{Vac}[Vac]}{K_{proteo}^{Vac}+[Vac]}Vol_{follicle}\frac{1.6}{2.6}[I_{Tg}] \\
\frac{\mathrm{d}}{\mathrm{d}t}I_{MD} &= \mathcal{S}_{proteo}^{Lys}\frac{V_{proteo}^{Vac}[Vac]}{K_{proteo}^{Vac}+[Vac]}Vol_{follicle}\frac{1}{2.6}[I_{Tg}].
\end{aligned}$$

[3] Square brackets denote concentration; e.g., $[I_S]$ is the concentration of plasma iodide, I_S.

3.2. Key biochemicals pools

These pools describe the dynamics of biochemicals taking part in hormone synthesis. These include the protein *NIS* which help transport iodide across the basolateral membrane into follicular cells; Hydrogen Peroxide H_2O_2, Thyroglobulin *Tg*, and Thyroid Peroxidase *TPO* which all participate in the formation of iodinated thyroglobulin; the effective content of thyroglobulin available for iodination Tg_{eff}; the colloidal droplets *Vac* transported into cells via endocytosis; and the lysosomes *Lys* participating in proteolysis.

$$\frac{\mathrm{d}}{\mathrm{d}t}NIS = \mathcal{S}^{SSF}_{NIS}\frac{\alpha^{I_F}_{NIS}}{K^{I_F}_{NIS}+[I_F]}\frac{\alpha^{Tg}_{NIS}}{K^{Tg}_{NIS}+[Tg]}scale - \frac{\tau^{NIS}_{decay}}{\frac{\tau^{I_F}_{decay}}{K^{I_F}_{decay}+[I^2_F]}}[NIS]$$

$$\frac{\mathrm{d}}{\mathrm{d}t}H_2O_2 = \alpha_{H_2O_2}\mathcal{S}^{SSF}_{apical}\frac{A_{apical,nom}scale}{A_{apical}}\frac{1+[I_C]_{nom}}{1+[I_C]^3} + 1000 - \tau^{H_2O_2}_{decay}[H_2O_2]^2 - \tau^{TPO}_{turnover}[TPO]\frac{V^{H_2O_2}_{org}[H_2O_2]}{K^{H_2O_2}_{org}+[H_2O_2]}\frac{V^{I_C}_{org}[I_C]}{K^{I_C}_{org}+[I_C]}\frac{V^{Tg_{eff}}_{org}[Tg_{eff}]}{K^{Tg_{eff}}_{org}+[Tg_{eff}]}$$

$$\frac{\mathrm{d}}{\mathrm{d}t}Vac = \mathcal{S}^{SSF}_{apical}\alpha_{endo}\frac{A_{apical}}{A_{apical,nom}} - \mathcal{S}^{Lys}_{proteo}\frac{V^{Vac}_{proteo}[Vac]}{K^{Vac}_{proteo}+[Vac]}Vol_{follicle}$$

$$\frac{\mathrm{d}}{\mathrm{d}t}Tg = \mathcal{S}^{SSF}_{Tg}\frac{\alpha^{Tg}_{Tg}}{K^{Tg}_{Tg}+[Tg]}scale - \mathcal{S}^{SSF}_{apical}\alpha_{endo}\frac{A_{apical}}{A_{apical,nom}}[Tg]$$

$$[Tg_{eff}] = \left(1-\frac{[I_{Tg}]}{[Tg]}\right)[Tg]$$

$$[TPO] = \mathcal{S}^{SSF}_{TPO}\frac{Vol_{colloid,nom}}{Vol_{colloid}}\frac{\alpha^{Tg}_{TPO}}{K^{Tg}_{TPO}+[Tg]}scale$$

$$[Lys] = \mathcal{S}^{SSF}_{Lys}\frac{Vol_{follicle,nom}}{Vol_{follicle}}\ scale.$$

3.3. Cell volume

This group of equation describe the scaling of the thyroid's physical size. The passive scaling parameter *scale*, based on age and weight, determines the number of follicle cells, while the dynamic scale-parameter *size*, based on $[TSH]$ and $[I_F]$ concentrations, determines the surface area and volume of a follicle cell and the colloid,

$$scale = \frac{Vol_{measured} - 0.17(1.97 + 0.21\ \text{weight} + 0.06\ \text{age})}{1.97 + 0.21\ \text{weight} + 0.06\ \text{age}}$$

$$\frac{\mathrm{d}}{\mathrm{d}t}size = \tau^{-1}_{size}\left(-size + \mathcal{S}^{SSF}_{cell}\mathcal{I}^{I_F}_{cell}\right).$$

3.4. Signal transduction

This group of equations describes the TSH-transduction pathway-gains which affect intracellular bio-processes.

$$[SSF] = \frac{100[TSH - R][TSH]}{178.2 + [TSH]}, \quad \mathcal{S}^{Lys}_{proteo} = \frac{V^{Lys}_{proteo}[Lys]}{K^{Lys}_{proteo} + [Lys]},$$

$$\mathcal{S}^{SSF}_{NIS} = \frac{V^{SSF}_{NIS}[SSF]}{K^{SSF}_{NIS} + [SSF]}, \quad \mathcal{S}^{SSF}_{TPO} = \frac{V^{SSF}_{TPO}[SSF]}{K^{SSF}_{TPO} + [SSF]},$$

$$\mathcal{S}^{SSF}_{Tg} = \frac{V^{SSF}_{Tg}[SSF]}{K^{SSF}_{Tg} + [SSF]}, \quad \mathcal{S}^{SSF}_{Lys} = \frac{V^{SSF}_{Lys}[SSF]}{K^{SSF}_{Lys} + [SSF]},$$

$$\mathcal{S}^{SSF}_{cell} = 0.81 + \frac{V^{SSF}_{cell}[SSF]}{K^{SSF}_{cell} + [SSF]}, \quad \mathcal{I}^{I_F}_{cell} = \frac{\alpha^{I_F}_{cell}}{K^{I_F}_{cell} + [I_F]},$$

$$\mathcal{S}^{SSF}_{apical} = \frac{V^{SSF}_{apical}[SSF]}{K^{SSF}_{apical} + [SSF]}.$$

4. Analysis, simulations, and discussion

In this section, using analysis and simulations, we highlight specific pathways that enable the thyroid to maintain desired hormonal secretion in the face of daily variations in iodine intake I_{in}. We model the thyroid as a bio-system operating at two levels [28]. The first level describes the thyroid's function in the overall HPT-axis dynamics (see Fig. 1). In this capacity, the thyroid secretes hormones in response to stimulation by TSH which is dependant on circulating thyroid hormones level. The second level involves the gland's feedback mechanisms that regulate iodide pools, often referred to as the thyroid's iodide autoregulation. Within this level, the thyroid's hormone secretion rate is robust to changes in dietary iodine intake.

We begin our analysis by computing the linearized input–output relations; i.e., transfer functions, between the thyroid's two inputs, $[TSH]$ and I_{in}, and its output, the secretion rate of hormonal iodide $\dot{I_H}$. We demonstrate that the transfer function from $[TSH]$ and $\dot{I_H}$ is essentially a constant, while the transfer function from I_{in} to $\dot{I_H}$ has a low-pass filter characteristics.[4] We then analyze the role of the cascaded inhibition feedback pathways in the overall operation of the gland as shown in Fig. 6. In this cascaded structure, each iodide pool feeds the next downstream pool while inhibiting accumulation of its immediate upstream pool. These cascaded signaling and inhibition pathways allow the iodide pool furthest away from the basolateral membrane, both spatially and metabolically, to regulate iodide uptake based on its current state (see Simulation 1).

Our analysis is augmented with simulations aimed at: (Simulation 1) supporting the findings from our analysis using time responses of intrathyroidal pools to dynamic TSH and I_{in} signals,

[4] By 'low-pass characteristic' we refer to the relative attenuation of the steady-state response of $\dot{I_H}$ to high-frequency sinusoidal inputs I_{in}.

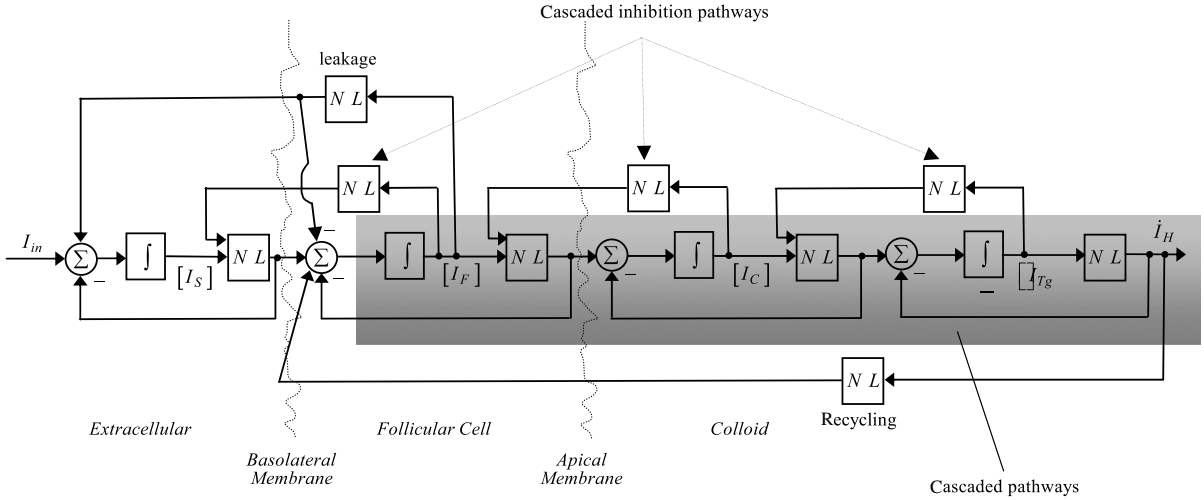

Fig. 6. A block diagram of the thyroid overall feedback structure (NL denotes a non-linear function and $\sum$ denotes a summer).

(Simulation 2) studying intracellular adaption during iodine deficiency, and (Simulation 3) applying the model as a hypothesis-testing tool to proposed mechanisms for explaining the thyroid's escape from the Wolff–Chaikoff block.

4.1. Linear Analysis

The thyroid gland is a dynamical system with two inputs, [TSH] and I_{in}, and an output, the rate of secreted hormonal iodide $\dot{I}_H$. We analyze the input–output behavior of the thyroid by first linearizing the model[5] and considering two cases: the baseline gland and a thyroid where the cascaded inhibition pathways are opened. In this latter case, the downstream pools no longer dynamically inhibit upstream pools (see Fig. 6). We examine steady-state and dynamic properties of the two cases. For simplicity we retain the same notation for the linearized states. The analysis and simulations are based on a euthyroid, 35-year-old human, weighing 72.6 kg with a total thyroid volume of 19.3 ml, ingesting the USA average of 160 μg of dietary iodine daily [30], and with a nominal [TSH] of 1.8 mU/dL.

We start our analysis by considering the frequency response[6] between the input (command) signal $[TSH]$ and the gland's hormonal secretion rate $\dot{I}_H$ shown in Fig. 7 (top). A constant amplitude

[5] We use MATLAB's Simulink package [29] to numerically simulate and linearize the model described in Section 3.

[6] The frequency response technique is a standard tool in engineering for analyzing the dynamics of systems (e.g., [31]). The frequency response of the linearized thyroid model is defined as the steady-state response of the output signal $\dot{I}_H$ to sinusoidal input signals I_{in} and $[TSH]$. At steady-state, the output signal oscillates at the input signal's frequency, but with a different amplitude and phase at each given frequency. For analysis purposes, we plot the amplitude ratio between an output and an input signal vs. a logarithmic frequency scale ('lower' frequencies denote 'slower' input signals). When this amplitude ratio drops at increasing frequencies we say that the corresponding system has low-pass dynamics, that is, it attenuates the faster input signals, relatively speaking.

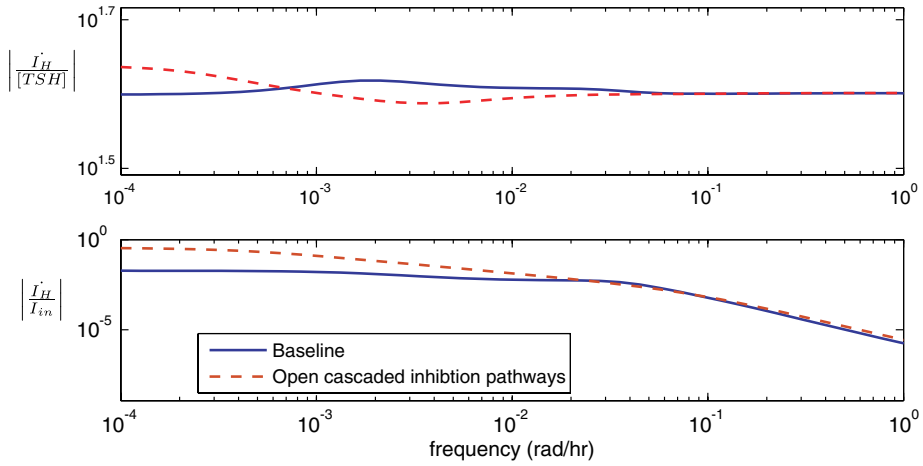

Fig. 7. Frequency responses of the thyroid from its input signals, $[TSH]$ and (top) and I_{in} (bottom), to its output signal, $\dot{I}_H$ in baseline and opened cascaded inhibition pathways cases.

ratio is seen over the entire frequency range in both the baseline and opened inhibition pathways cases. We draw two conclusions about the properties of the thyroid as a subsystem in the overall HPT-axis dynamics: (1) the cascaded inhibition pathways have little effect on the overall dynamics between TSH and hormonal secretion rate, and (2) the thyroid responds equally well to TSH signals over all time scales such as constant, periodic (circadian) and fast (pulsatile) commands. The dynamic between TSH command and hormonal secretion rate is constant, and this is consistent with previously reported quantitative analysis in [12,13].

The frequency response from iodine intake I_{in} to the gland's secretion rate $\dot{I}_H$ provides a key insight into the thyroid's iodide autoregulation mechanisms (Fig. 7, bottom). In spite of variation in iodide intake, there is little evidence to suggest it has appreciable effect on the thyroid's secretion rate. The responses for both the baseline and opened inhibition pathways cases exhibit low-pass filter characteristics. That is, the effects of changes in iodine intake, other than in mean value, will be attenuated and have little effect on the thyroid hormonal secretion rate. A plausible explanation for this has to do with the intrathyroidal iodide pools comprising the fabric of iodide flow pathways through the basolateral membrane into the colloid. The two smaller inorganic iodide pools, $[I_F]$ and $[I_C]$, unlike the third, large organic iodide pool $[I_{Tg}]$, are able to quickly react to 'fast' variations in uptake levels and propagate their state into the next downstream pool and immediate upstream pool.

The cascaded inhibition pathways play a crucial role in the thyroid's robustness to changes in mean iodine intake values. In order to take into account the relative amplitudes of the input/output signals we normalize each by its nominal value: $(\dot{I}_H)_N = 74.87^{-1}\dot{I}_H$, $([TSH])_N = 1.8^{-1}[TSH]$, and $(I_{in}^-)_N = 160^{-1}I_{in}^-$. The resulting normalized relations are shown in Table 1. In the baseline case, we see that $(\dot{I}_H)_N$ tracks constant $([TSH])_N$ inputs very well, with only a 0.5% error, while, at the same time, attenuating constant changes to $(I_{in})_N$ inputs by a factor of almost 25! However, in the second case, when the cascaded inhibition pathways are opened, changes in the thyroid's secretion rate $(\dot{I}_H)_N$ are quite sensitive to constant changes in $(I_{in})_N$, where a 1% change in $(I_{in})_N$ results in a 0.744% change in $(\dot{I}_H)_N$.

Table 1
Normalized, input–output relations for constant inputs for the baseline case and the case when the cascaded inhibition pathways are opened

Case	Normalized relations
Baseline	$(\dot{I_H})_N = 0.955([TSH])_N - 0.041(I_{in})_N$
Opened cascaded inhibition pathways	$(\dot{I_H})_N = 1.057([TSH])_N + 0.744(I_{in})_N$

4.2. Simulations

Next, based on the non-linear model, we present three time simulations to illustrate the gland's response at different physiological conditions. The first simulation shows the gain-like nature of the input–output response from TSH command to secretion rate response $\dot{I_H}$. It also shows the response of the intrathyroidal iodide pools. The second simulation explores the intrathyroidal adaptations occurring as a result of a dietary iodine deficiency. The third simulation demonstrates the model's power as an hypothesis-testing tool.

Simulation 1. In this simulation we investigate the thyroid's ability to maintain stable hormonal secretion in the face of daily changes in iodine intake I_{in}. Our TSH signal has a 1.8 mU/dL mean, a circadian (modeled using a sinusoid), and 13 pulses a day [32] components. The pulses' events are random with uniform distribution while their amplitudes are normally distributed. Changes in daily dietary iodine are modeled using a normally distributed random signal with mean equal to the USA average of 160 μg [30] and variance of 10^3.

The preceding analysis showed a gain-like pathway between [TSH] and $\dot{I_H}$ is confirmed by the simulation results in Fig. 8. The hormonal secretion rate $\dot{I_H}$ closely matches the circadian and pulsatile characteristics of command signal $[TSH]$. Also confirmed is the low-pass nature of the transfer function from I_{in} to $\dot{I_H}$; the noisy iodide intake levels have negligible effect on $\dot{I_H}$. The cascaded signaling pathways (highlighted in Fig. 6), in which inorganic iodide flows from blood to follicle to colloid, collectively and effectively serve as a series of low-pass filters. These iodide pools (Fig. 9) show the affects of successive 'smoothing', which eventually results in a near constant $[I_{Tg}]$ pool.

Simulation 2. The gland's iodide autoregulation mechanism and its extracellular fluid (ECF) feedback system (see Appendix A for a description of this ECF mechanism) continuously adapt to maintain stable hormonal secretion rates in the face of changing iodine intake level. When the changes become sufficiently large, the adaptation's effectiveness diminishes and the HPT-axis will modify the TSH command level. To exercise this dynamic, we repeat the conditions of Simulation 1, but for simplicity consider constant TSH and remove the noise from I_{in}. We first run the simulation for 10 effective days to reach equilibrium. At hour 240 we reduce the dietary iodine intake level from 160 μg/day to 100 μg/day. Fig. 10 shows that the feedback mechanisms are unable to fully adapt, with the secretion rate decreasing to 3 μg/h, slightly below the desired value of 3.12 μg/h. Details of the adaptation mechanisms can be observed in Figs. 11 and 12. The gland, following the initial transients, raises its iodide uptake levels while sharply reducing iodide leakage back into ECF. Simultaneously, at the ECF feedback level, urine iodide clearance is reduced to match the reduced intake level. The low-pass characteristic of the gland results in a minimal $\dot{I_H}$

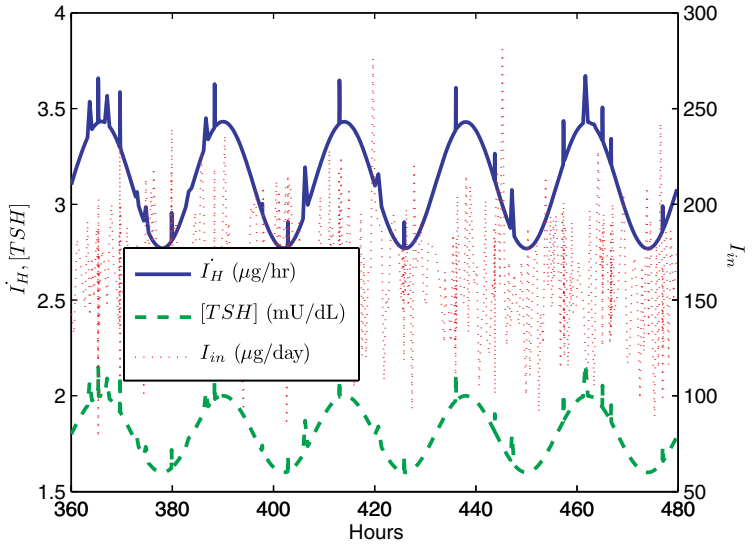

Fig. 8. Inputs (TSH and iodine intake) and output (hormonal iodide secretion rate) in Simulation 1.

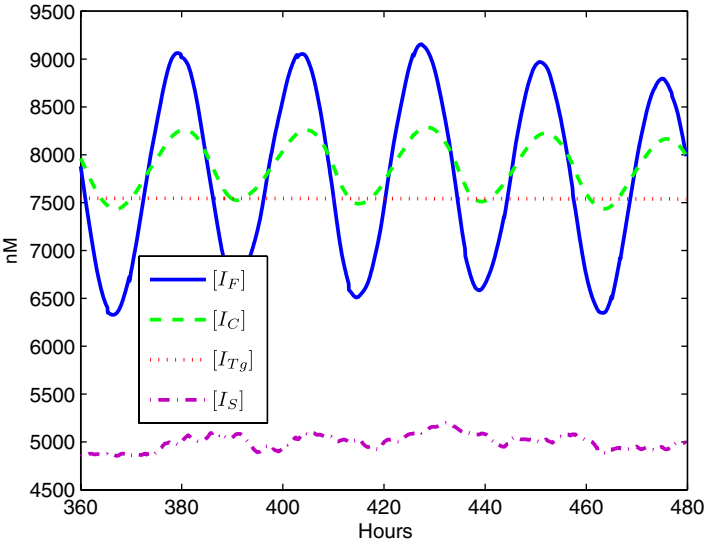

Fig. 9. Iodide pools in Simulation 1.

decrease, however, it is also responsible for the long time constants, taking weeks for the iodide pools (Fig. 12) to reach steady state. We emphasize that this adaptation occurs independent of TSH stimulation since the $[TSH]$ command is constant throughout the simulation. Hence, it becomes necessary for the HPT-axis to marginally increase TSH in order to command the gland back to a normal secretion rate. Indeed, when $[TSH]$ is slightly increased to 1.9 mU/dL, iodide secretion rate $\dot{I}_H$ is recovered to 3.12 μg/h.

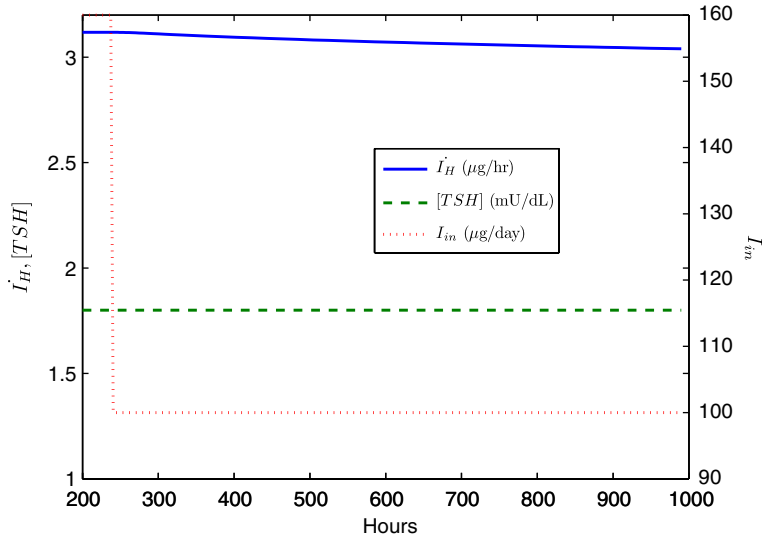

Fig. 10. Inputs (TSH and iodine intake) and output (hormone iodide secretion rate) under reduction in dietary iodine intake at 240 h in Simulation 2.

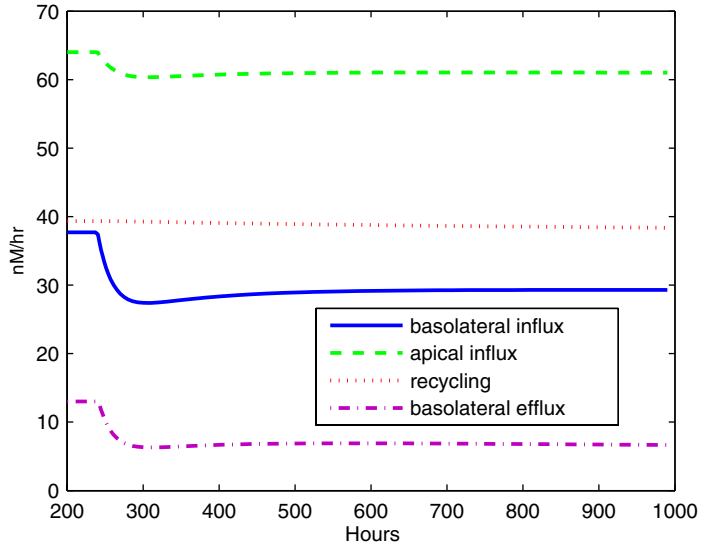

Fig. 11. Follicle cell iodide fluxes under reduction in dietary iodine intake at 240 h in Simulation 2 (see Appendix A for details about these iodide fluxes).

Simulation 3. Section 2.3 described the thyroid response to high doses of iodine intake – the Wolff–Chaikoff block and escape. High doses of iodine intake block iodide organification within hours, however, normal organification resumes as early as two days later. The exact mechanisms underlying the escape are yet to be fully established. A recent review of NIS research [33] remarked that 'Whether the different results concerning NIS regulation by iodide at a transcrip-

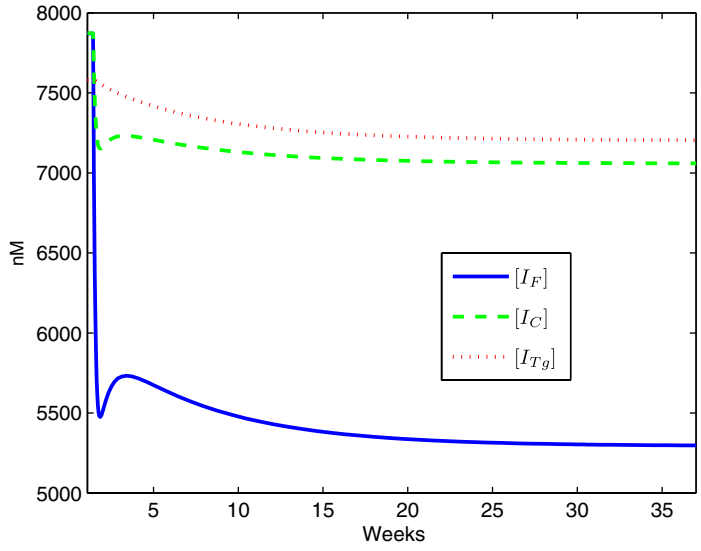

Fig. 12. Intrathyroidal iodide pools in dietary iodine intake at 240 h in Simulation 2.

tional and/or post-transcriptional level are due to different experimental conditions is something that needs to be clarified'. Several studies have investigated this phenomena. One study has suggested that the escape is due to a decrease in NIS expression [25], while another study reported a reduction in NIS protein levels with no decrease in NIS mRNA levels [26]. Other recent studies have reported a 50% decrease in both iodide uptake and NIS mRNA levels [34], supporting the hypothesis that reduced expression of NIS [35] is involved in escape from the Wolff–Chaikoff block. Our next simulation was designed to study two competing hypotheses for this escape; i.e., whether it is production (translation and/or transcription) or degradation (post-translation) that is responsible for escape. The simulation serves as a demonstration of the model's utility as hypothesis testing tool.

The physiological conditions in this simulation are the same as those in Simulation 2, however, at day 10 there is an acute surge of dietary iodine intake level from 160 μg/day to 1500 μg/day. Excess plasma iodide is presently modeled (baseline model) to affect the thyroid on the basis of both hypotheses above. It inhibits NIS production and increases NIS degradation according to (see Section A.4):

$$\textbf{Baseline}: \frac{\mathrm{d}}{\mathrm{d}t}NIS = \underbrace{\mathcal{S}_{NIS}^{SSF}\underbrace{\frac{\alpha_{NIS}^{I_F}}{K_{NIS}^{I_F}+[I_F]}}_{\text{inhibition}}\frac{\alpha_{NIS}^{Tg}}{K_{NIS}^{Tg}+[Tg]}scale_{\text{production}}}_{} - \underbrace{\frac{\tau_{decay}^{NIS}}{\frac{\tau_{decay}^{I_F}}{K_{decay}^{I_F}+[I_F^2]}}}_{\downarrow\text{half-life}}[NIS]_{\text{degradation}}.$$

To study the hypothesis (Hypothesis A) that inhibition of NIS production is responsible for the escape, we model a more aggressive inhibition term using an $[I_F]^5$ dependance:

Hypothesis A.

$$\frac{\mathrm{d}}{\mathrm{d}t}NIS = \mathcal{S}_{NIS}^{SSF}\frac{\alpha_{NIS}^{I_F}}{K_{NIS}^{I_F}+[I_F]^5}\frac{\alpha_{NIS}^{Tg}}{K_{NIS}^{Tg}+[Tg]}scale - \frac{\tau_{decay}^{NIS}}{\frac{\tau_{decay}^{I_F}}{K_{decay}^{I_F}+[I_F^2]}}[NIS],$$

while the hypothesis (Hypothesis B) that increased degradation is responsible for the escape is modeled by maintaining a constant half-life according to

Hypothesis B.

$$\frac{\mathrm{d}}{\mathrm{d}t}NIS = \mathcal{S}_{NIS}^{SSF}\frac{\alpha_{NIS}^{I_F}}{K_{NIS}^{I_F}+[I_F]}\frac{\alpha_{NIS}^{Tg}}{K_{NIS}^{Tg}+[Tg]}scale - \tau_{decay}^{NIS}[NIS].$$

We conducted simulations with these three model variations: a baseline model, a sharper inhibition of NIS production model, and fixed degradation model. Since it was parameterized to achieve this dynamic, the baseline model simulation exhibits the expected transients: a 2-h block and a corresponding 2-day escape; see Figs. 13 and 14. We were surprised to discover that little can be gained with the sharper inhibition of NIS production model. Other than minimal differences in steady-state values, similar transients to baseline model were observed. The model with a fixed degradation term results in significantly slower NIS adaptation with the escape occurring much later (>10 days). While the particular molecular mechanisms involved in NIS production inhibition and increased degradation of NIS are not well understood, this simulation supports the hypothesis that some form of post-translational process is mostly responsible for the Wolff–Chaikoff escape from an acute surge of dietary iodine intake. This is summarized in Table 2.

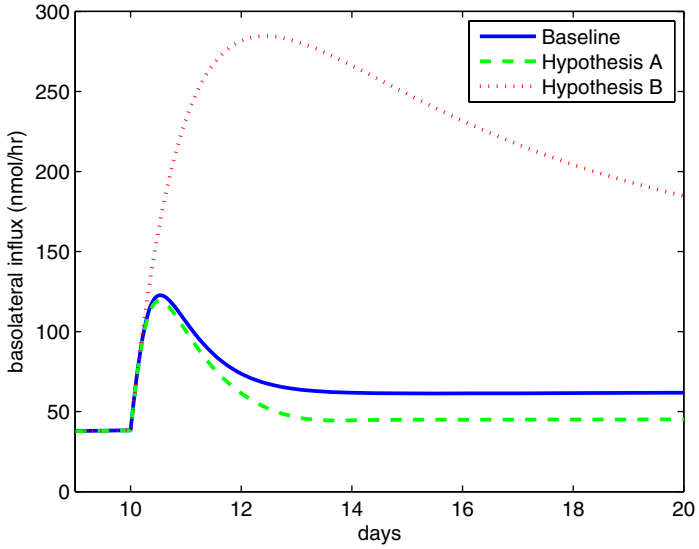

Fig. 13. Basolateral influx rates corresponding to three hypothetical NIS models following a surge in dietary iodine at day 10 in Simulation 3.

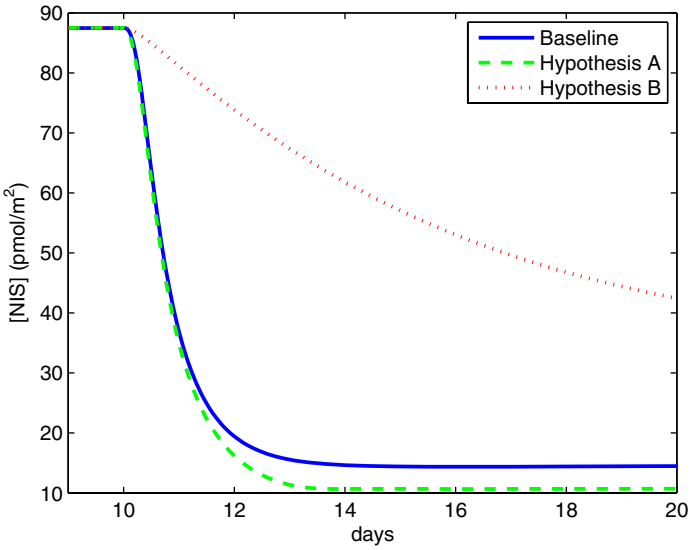

Fig. 14. NIS concentrations corresponding to three hypothetical NIS models following a surge in dietary iodine at day 10 in Simulation 3.

Table 2
Testing the two hypotheses related to the Wolff–Chaikoff escape

	Baseline	Hypothesis A	Hypothesis B
Escape within	2 days	2 days	>10 days

5. Conclusions

This paper presents a computational model of the human thyroid which captures many aspects of thyroid cell biology. Our analysis of the model's feedback structure validates clinical observations that the thyroid's response to the HPT-axis command signal TSH is robust with respect to varying dietary iodine intake levels. At the core of the gland's feedback system is a large storage of iodinated thyroglobulin and cascaded inhibition pathways that play a key role in achieving this robustness. This model provides a first step in establishing a quantitative understanding of the integrated control systems involved in thyroid hormone metabolism. This model may provide an important tool for the study of normal and diseased thyroid behavior, its reaction to environmental contaminants such as perchlorate, and effects of new therapeutic protocols with patient-specific modeling.

Acknowledgments

This material is based upon work supported in part by the National Science Foundation (NSF) under Grant No. 0556081. Any opinions, findings and conclusions or recommendations expressed in this material are those of the author(s) and do not necessarily reflect the views of the NSF.

Appendix A. Modeling details

In this appendix we present a set of non-linear differential equations describing the thyroid model as depicted in Fig. 5. The presentation focuses initially on a single follicle, then generalizes the single cell into a whole-thyroid model. We primarily used quasi steady-state Michaelis–Menton enzyme kinetics. This class of sigmoidal relations, characterizing of many signaling cascades, is commonly used to describe transport, stimulation/promotion/activation, and inhibition processes (e.g., [36]). A sigmoidal relation is also used to describe degradation/clearance dynamics similarly to its use in pharmacokinetics to model elimination rate of drug from a pool [37]. We also use a generalization of the sigmoidal relation, the so-called four-parameter sigmoidal relation (e.g., [38]). In summary, the equations and parameters comprising our model reasonably describe the quantitative nature input–output dynamics between various biochemicals, although they often oversimplify the underlying dynamics. Finally, our time variable has been scaled from seconds to hours. Next, we describe top-level dynamics of the iodide pools and then move to a more detailed explanation.

A.1. Main iodide pools

Here we model the transport of the organic and inorganic iodide pools in Fig. 5. Combining the influx and efflux terms for the follicular cell, the dynamics of its inorganic iodide pool I_F is given by mass action

$$\frac{\mathrm{d}}{\mathrm{d}t} I_F = \text{basolateral influx} + \text{reccyling influx} - \text{basolateral efflux} - \text{apical influx}.$$

Similarly, the inorganic iodide pool dynamics within the colloid can be described by

$$\frac{\mathrm{d}}{\mathrm{d}t} I_C = \text{apical influx} - \text{endocytosis}[I_C] - \text{organification}.$$

Once transported into the colloid, iodide is organified and incorporated into Tg, and the dynamic of its pool within the thyroglobulin molecule is given by

$$\frac{\mathrm{d}}{\mathrm{d}t} I_{Tg} = \text{organification} - \text{endocytosis}[I_{Tg}].$$

Being a relatively stable molecule, Tg is assumed here to be lost through endocytosis at a much faster rate than it degrades. In what follows, we detail the processes and variables involved in the above iodide pools.

A.2. Auxiliary iodide pools

In addition to the main iodide pools described in Section A.1, additional pools are needed to capture iodide content in hormone precursors and secreted hormones. In a reaction catalyzed by TPO, the iodinated tyrosyl residues within thyroglobulin are 'coupled' to form thyroid hormone precursors. The state I^*_{MD} is used to indicate the concentration of organic iodide bound to iodotyrosyl precursors within the colloid. It will be paired with a second state, I^*_H, which is

the concentration of organic iodide bound to thyroid hormone precursors within the colloid. That is, the total amount of organic iodide attached to Tg is $I_{Tg} = I^*_{MD} + I^*_H$. Hence, the dynamics of iodide bound to iodotyrosol precursors is described by

$$\frac{\mathrm{d}}{\mathrm{d}t} I^*_{MD} = \text{organification} - \text{coupling} - \text{endocytosis}\left[I^*_{MD}\right],$$

and the dynamics of organic iodide bound to thyroid hormone precursors is described by

$$\frac{\mathrm{d}}{\mathrm{d}t} I^*_H = \text{coupling} - \text{endocytosis}\left[I^*_H\right].$$

Following proteolysis, DIT and MIT are immediately attacked by iodotyrosine-specific deiodinase in the cytoplasm, a process that reclaims their iodide and tyrosyl residue for future use in hormone synthesis. The formation of MIT and DIT is a function of the proteolysis and the concentration of iodotyrosine precursors within thyroglobulin [23]. Putting everything together, the dynamics of organic iodide bound to MIT and DIT can be described by

$$\frac{\mathrm{d}}{\mathrm{d}t} I_{MD} = \text{proteolysis}\left[I^*_{MD}\right] - \text{recycling influx}.$$

The flow rate of thyroid hormones from proteolysis depends also upon the composition of the contents of the vacuoles. The rate of hormone synthesis is therefore the same as the rate of proteolysis, multiplied by the concentration of hormone precursors. The dynamics of hormone iodide synthesis is therefore described by

$$\frac{\mathrm{d}}{\mathrm{d}t} I_H = \text{proteolysis}\left[I^*_H\right].$$

A remark is in order here. It has been reported that MIT:DIT and $T_3 : T_4$ ratios in iodinated thyroglobulin vary under different physiological conditions [39]. In this paper we are concerned with the aggregate flows of iodide and assume that I^*_{MD} and I^*_H are fixed ratios of I_{Tg}, hence the above equations for $\frac{\mathrm{d}}{\mathrm{d}t} I^*_{MD}$ and $\frac{\mathrm{d}}{\mathrm{d}t} I^*_H$ and the coupling relation described later are not used here. Also, in addition to T_3 and T_4, the gland produces and secretes rT_3, a non-biologically active form of the hormone. We ignore rT_3 in our model of iodide metabolism for an average, euthyroid state. In other thyroid states and when accurate concentrations are of interest, the variability of MIT:DIT and $T_3 : T_4$ ratios in iodinated thyroglobulin and rT_3 must be accounted for.

A.3. Iodide transport

TSH stimulation. When TSH binds to its receptor on the cell surface of the thyroid, it causes the activation of different internal signal pathways within the thyroid [20] as described earlier. The in-vivo concentrations of these messenger molecules are not well described. Hence, their aggregate behavior is modeled using a single, non-dimensionalized state, SSF, by equating their normal equilibrium concentrations with the value of 1. Also, since these signals are short lived (on the order of seconds [40]) relative to the model's time scale of hours, the dynamics between TSH and the secondary messengers can be neglected and simplified to a saturable gain relation. The concentration of the secondary messenger signal is described by a hyperbolic relation, with influence by TSH-R

$$[SSF] = \frac{100[TSH - R][TSH]}{178.2 + [TSH]}.$$

Given the limited quantitative data on $[TSH - R]$, we lump this protein and the hormone-ligand relation using a fixed value of $[TSH - R] = 1$.[7] Under euthyroid physiological conditions of $[TSH] = 1.8$ mU/dL we have $SSF = 1$. The above choice of a 100-fold increase between the nominal condition and the maximum stimulation state $[SSF]$ is not unique but it allows for sufficient gain in the biosynthetic pathways to model abnormal states such as hyperthyroidism.

Basolateral influx. The principal entry point of iodide into the thyroid follicle cells is through the membrane glycoprotein known as the Na^+/I^- Symporter which has been well characterized in recent years ([19,41]). It uses the concentration gradient of Na^+ (high in plasma, low in cell) to drive up I^- up its concentration gradient into the thyroid, creating a concentration 20-40 times that in the blood [42]. The Na^+ is then returned to the plasma via Na^+/K^+ ATPase. We assume that plasma concentrations of Na^+, K^+, and Na^+/K^+ ATPase remain fixed relative to the two inputs in question, TSH and plasma iodide, so that their relative contributions to the dynamics can be neglected.[8] The parameters of the NIS molecule found in [19,41] are used in our model.[9]

Iodide binds the NIS molecule in a manner similar to an enzyme-substrate relationship, with the product being iodide on the interior of the cell membrane. As such, a Michaelis–Menton kinetics is used to describe the relationship with I_S the substrate and NIS acting as the enzyme. The basolateral iodide influx model is described by

$$\text{basolateral influx} = \frac{K^{NIS}_{turnover}[NIS][I_S]}{K^{NIS}_m + [I_S]} A_{basal}.$$

Recycling influx. The concentration of intracellular inorganic iodide is also affected by breakdown of waste products (MIT and DIT) of thyroglobulin proteolysis. The transmembrane protein Iodotyrosine dehalogenase 1 (DEHAL1) is involved in this recycling of iodide [43] which is dependant upon the concentrations of MIT and DIT within the cell [23]. The proportion between the two molecules is assumed to be constant, as is that of D1.[10] The recycling rate relation is described by

$$\text{recycling influx} = \frac{V^{I_{MD}}_{rec}[I_{MD}]}{K^{I_{MD}}_{rec} + [I_{MD}]} Vol_{follicle}.$$

[7] The secondary messenger pathways have very little effect on the transcription of TSH-R [20].

[8] The motivation behind this assumption is as follows: considering Na^+, K^+, and Na^+/K^+ ATPase having the role of enzymes in an enzyme-substrate kinetics, they can be neglected in Michaelis–Menton kinetics if their quantities are assumed much larger than that of the substrate as is the situation here.

[9] While these numbers were actually for a rat thyroid NIS expressed in frog (*Xenopus leavis*) oocytes, comparative physiological research has shown that NIS behavior is similar throughout the mammalian class [41]. Kinetic data for human NIS is not available in sufficient detail.

[10] It may be of interest to model a separate D1 pool that is inhibited by low thyroid hormone levels [44] to study the effect of the dehalogenase defect [45,46]. However, it is outside the scope of this paper.

Basolateral efflux. Inorganic iodide leaves the cell through the basal membrane by flowing down its concentration gradient, back into the plasma [16]. This rate depends on the concentration of inorganic iodide within the thyroid cell and the surface area available for diffusion. Based on our simulation studies, a second-order diffusion rate law appears to adequately model the dynamics seen in the Wolff–Chaikoff block and escape,

$$\text{basolateral efflux} = \alpha_{dif}^{I_F}[I_F]^2 A_{basal}.$$

Apical influx. Inorganic iodide also leaves the cell through the apical membrane. The apical iodide transport is understood less than basolateral transport. There is current debate about the actual molecule involved in the transport, with the leading contenders being Apical I^- Transporter (AIT) [47] and Pendrin [48]. We model the apical transport using two separate channels, with affinity constants K_{m1}^{apical} and K_{m2}^{apical}, respectively, with $K_{m1}^{apical} \ll K_{m2}^{apical}$ [49]. As an integral part of the biosynthetic pathway, this process is also believed to be stimulated by the secondary messenger signal [50].

As described earlier, excess intrathyroidal iodide has an inhibitory effect on a number of processes (Wolff–Chaikoff block and escape). Apical membrane transport must be slowed down in the event of high iodide levels in the colloid. Without this effect, excess iodide would simply continue accumulate in the colloid. Whether this inhibition is due to a loss of the electrochemical gradient between the follicle and the colloid or a negative feedback on the transport protein does not matter for the purposes of this model. Therefore, the apical transport function must include an inhibition term to account for rise in colloidal inorganic iodide concentration. Combining this inhibition with the basic transport mechanism, the apical rate equation is described by

$$\text{apical efflux} = \mathcal{S}_{apical}^{SSF} \frac{\alpha_{apical}^{I_C}}{K_{apical}^{I_C} + [I_C]^3} \left(\frac{V_1^{apical}[I_F]}{K_{m1}^{apical} + [I_F]} + \frac{V_2^{apical}[I_F]}{K_{m2}^{apical} + [I_F]} \right) A_{apical},$$

where $\mathcal{S}_{apical}^{SSF}$ denotes the stimulatory effect of secondary signal messenger on transport and where

$$\mathcal{S}_{apical}^{SSF} = \frac{V_{apical}^{SSF}[SSF]}{K_{apical}^{SSF} + [SSF]}.$$

Again, while not supported by specific known mechanisms, our simulations indicated the need for a sharp inhibition $[I_C]^3$ term above the achieve a 2-h Wolff–Chaikoff block.

Organification. Upon arrival at in the colloid, iodide is oxidized by H_2O_2, catalyzed by TPO, and incorporated into the tyrosyl residues within thyroglobulin [16]. This entire reaction cannot proceed without the raw material I^- and the compounds that operate on the raw material, H_2O_2 and TPO. It is modeled as a Michaelis–Menton kinetics with TPO as the enzyme, linearly affecting the velocity term, forming a complex with the three substrates I^-, H_2O_2, and Tg, resulting in organification of iodide. Tg, I^-, and H_2O_2 (consumed in the reaction) also behave like substrates.

There are a finite number of iodide binding sites within each molecule of thyroglobulin. Thus, as Tg becomes more and more iodinated, it becomes increasingly difficult to organify iodide [22]. Organification will therefore be inhibited by a high organic iodide concentration. Furthermore, the entire Tg molecule does not react in the organification reaction.[11] At

[11] Only selective binding sites are available for iodination, with the maximum number of atoms of iodide that a single thyroglobulin molecule can accommodate has been measured to be around 57 atoms per molecule [22].

higher levels of iodination the thyroglobulin is insoluble and forms isolated globules that do not participate in biosynthesis. It is believed that this insoluble form is used for additional storage of iodide [23]. This overall effect can be modeled as a classical inhibition process. A new term, Tg_{eff}, is introduced to model the effective amount of thyroglobulin that is reacting in the organification process. Collecting the above, the rate of organification is described by

$$\text{organification} = \tau_{turnover}^{TPO}[TPO]\frac{V_{org}^{H_2O_2}[H_2O_2]}{K_{org}^{H_2O_2}+[H_2O_2]}\frac{V_{org}^{I_C}[I_C]}{K_{org}^{I_C}+[I_C]}\frac{V_{org}^{Tg_{eff}}[Tg_{eff}]}{K_{org}^{Tg_{eff}}+[Tg_{eff}]}.$$

Coupling. Once iodide has been added to the tyrosyl residues within the thyroglobulin molecule, it forms the precursors to the iodotyrosines MIT and DIT. It will either undergo coupling of the tyrosyl residues to form the precursor to thyroid hormone within the Tg molecule, or it will be transported out via endocytosis as MIT/DIT [51]. The coupling reaction can be modeled as a standard Michaelis–Menton equation with $[I_{MD}^*]$ as the substrate, $[TPO]$ as the enzyme, and $[I_H^*]$ as the product. The coupling kinetics is described by

$$\text{coupling} = \frac{\tau_{turnover}^{coupling}[TPO]\left[I_{MD}^*\right]}{K_{coupling}^{I_{MD}^*}+\left[I_{MD}^*\right]}Vol_{colloid}.$$

Endocytosis. Endocytosis is a fluid transport process [51] that is different from the chemical processes described so far. The vacuoles of endocytosis are formed by an invagination of the apical membrane, making the fluid contained in the vacuole identical to the fluid in the colloid at the time of invagination [51]. Putting everything together, a fluid transport equation, stimulated by TSH, is described by

$$\text{endocytosis} = \mathcal{S}_{apical}^{SSF}\alpha_{endo}\frac{A_{apical}}{A_{apical,nom}}.$$

Proteolysis. The mechanism of proteolysis is the fusion of vacuoles containing colloid material (from endocytosis) with lysosomes, and the subsequent breakdown of thyroglobulin [51]. The lysosomes contain digestive enzymes that cleave the tyrosyl residues from within the thyroglobulin molecule. The uncoupled residues form MIT and DIT and the coupled residues form T_3 and T_4. When a vacuole fuses with a lysosome and undergoes proteolysis, the fluid inside is not necessarily consumed. It does, however, cease to exist for the purposes of the biosynthetic pathway. Therefore, proteolysis is modeled as the processing and disappearance of the colloid-containing vacuoles, as a function of the concentration of lysosomes and vacuoles within the follicular cell,

$$\text{proteolysis} = \mathcal{S}_{proteo}^{Lys}\frac{V_{proteo}^{Vac}[Vac]}{K_{proteo}^{Vac}+[Vac]}Vol_{follicle},$$

where the stimulatory effect of lysosomes on proteolysis is described by

$$\mathcal{S}_{proteo}^{Lys} = \frac{V_{proteo}^{Lys}[Lys]}{K_{proteo}^{Lys}+[Lys]}.$$

A.4. Dynamics of biochemicals pools

Here we describe the governing relations for key biochemicals taking part in the biosynthesis of thyroid hormones.

Sodium/iodide symporter. Excess intrafollicular iodide inhibits NIS transcription [22]. This effect is an integral part of the thyroid's system of iodide autoregulation, allowing the thyroid to adapt to changing dietary iodine intake without requiring substantial changes in TSH levels [52]. Furthermore, thyroglobulin is fed back via the apical membrane-bound asialoglycoprotein receptor ASGPR to also inhibit transcription of NIS [27]. Hence, production of NIS can be described by

$$\text{NIS production} = \mathcal{S}_{NIS}^{SSF} \frac{\alpha_{NIS}^{I_F}}{K_{NIS}^{I_F} + [I_F]} \frac{\alpha_{NIS}^{Tg}}{K_{NIS}^{Tg} + [Tg]} scale,$$

where the variable *scale* is used to scale the thyroid size based on the age and weight (see Section A.6), and where the local stimulatory effect of TSH is described by the term2

$$\mathcal{S}_{NIS}^{SSF} = \frac{V_{NIS}^{SSF}[SSF]}{K_{NIS}^{SSF} + [SSF]}.$$

NIS has a half-life of 120 h [19], but this changes as larger $[I_F]$ has post-translational effect by increasing NIS degradation and/or detachment from the membrane [19]. This can be modeled as follows:

$$\text{NIS decay} = \frac{\tau_{decay}^{NIS}}{\frac{\tau_{decay}^{I_F}}{K_{decay}^{I_F} + [I_F^2]}} [NIS].$$

Combining the above results in the rate equation for NIS gives

$$\frac{\mathrm{d}}{\mathrm{d}t} NIS = \text{NIS production} - \text{NIS decay}.$$

In this model, the concentration of NIS is described based on its distribution on the surface area of the thyroid follicle. Being a membrane-bound transport protein, with the surface area A_{basal} changing with TSH and iodide levels, the effect of NIS on iodide uptake is reasonably modeled using this concentration,

$$[NIS] = \frac{NIS}{A_{basal}}.$$

Thyroid peroxidase. Production of TPO production is modulated by the secondary messenger pathways and is inhibited by Tg, via the ASGPR [27]. Due to its poorly understood in-vivo chemical kinetics, TPO concentration stimulated by TSH and Tg-inhibited (by the hyperbolic relation) is described by,

$$[TPO] = \mathcal{S}_{TPO}^{SSF} \frac{Vol_{colloid,nom}}{Vol_{colloid}} \frac{\alpha_{TPO}^{Tg}}{K_{TPO}^{Tg} + [Tg]} scale,$$

where the local stimulatory effects of TSH are described by

$$\mathcal{S}_{TPO}^{SSF} = \frac{V_{TPO}^{SSF}[SSF]}{K_{TPO}^{SSF} + [SSF]}.$$

Thyroglobulin. Production of Tg is modulated by the secondary messenger pathways and is self-inhibited via the ASGPR [27],

$$\text{Tg production} = \mathcal{S}_{Tg}^{SSF} \frac{\alpha_{Tg}^{Tg}}{K_{Tg}^{Tg} + [Tg]} scale,$$

where the local stimulatory effects of TSH are given by

$$\mathcal{S}_{Tg}^{SSF} = \frac{V_{Tg}^{SSF}[SSF]}{K_{Tg}^{SSF} + [SSF]}.$$

Being a relatively stable molecule, Tg loss via endocytosis dominates its degradation [53], hence, the latter is neglected so that

$$\frac{\mathrm{d}}{\mathrm{d}t} Tg = \text{Tg production} - \text{endocytosis}[Tg].$$

The organic iodide content of thyroglobulin can range from 0.1% to 1%, with normal being around 0.5% iodide by weight [23]. Kinetics of iodination of thyroglobulin by TPO has been measured with the affinity constant K_m^{TPO} and the turnover rate $\tau_{turnover}^{TPO}$ reported in [22]. The percent iodination of Tg is computed by,

$$\%\text{iodination} = 100 \frac{[I_{Tg}]}{[Tg]}.$$

The effective thyroglobulin variable can now be modeled as,

$$[Tg_{eff}] = \left(1 - \frac{\%\text{iodination}}{1\%}\right)[Tg].$$

Lysosomes. The secondary messenger pathways modulate lysosome production whose concentration is described by the hyperbolic relation,

$$[Lys] = \mathcal{S}_{Lys}^{SSF} \frac{Vol_{follicle,nom}}{Vol_{follicle}} scale,$$

where the local stimulatory effects of TSH are described by

$$\mathcal{S}_{Lys}^{SSF} = \frac{V_{Lys}^{SSF}[SSF]}{K_{Lys}^{SSF} + [SSF]}.$$

Hydrogen peroxide. The secondary messenger pathways increase production of H_2O_2 [22]. Excess intrathyroidal iodide is known to inhibit production [22], a phenomenon known as the Wolff–

Chaikoff Block. H_2O_2 is assumed to be affected by high levels of I_C since its production is located at the apical membrane surface where the effects of Wolff–Chaikoff are felt most acutely [54]. A 4-parameter sigmoidal relationship (e.g., [38]) was found using simulation to adequately model production and inhibition,

$$H_2O_2 \text{ production} = \alpha_{H_2O_2}\mathcal{S}^{SSF}_{apical}\frac{A_{apical,nom}scale}{A_{apical}}\frac{1+[I_C]_{nom}}{1+[I_C]^3}+1000.$$

Hydrogen peroxide is consumed by the organification of iodide [22], and any excess is quickly degraded by the cell as defense mechanism against this highly toxic product [54]. Both actions are combined into a second-order decay rate,

$$H_2O_2 \text{ decay} = \tau^{H_2O_2}_{decay}[H_2O_2]^2.$$

The rate at which H_2O_2 is consumed is calculated by using the rate of organification of iodide and a stoichiometric relationship of 1:1. Collecting all terms gives

$$\frac{d}{dt}H_2O_2 = H_2O_2 \text{ prduction} - H_2O_2 \text{ decay} - \text{organification}.$$

Vacuoles. The formation of vacuoles is a result of endocytosis, and their rate of disappearance is equal to the rate of proteolysis, giving

$$\frac{d}{dt}Vac = \text{endocytosis} - \text{proteolysis}.$$

A.5. ECF iodide pool

A minimal dynamic model of the extracellular fluid (ECF) iodide feedback mechanism is used here. This rudimentary model compared with the [5]) is sufficient here since we are interested only in the aggregate and not in the concentrations of iodide in specific pools such as in T_3 and T_4. Additional details about this iodide metabolism model can be found in [17]. The dynamics of plasma iodide pool are described using

$$\frac{dI_S}{dt} = I_{in} + \text{hormonal iodide recycling} + \text{basolateral efflux} - \text{basolateral influx} - \text{urineclearance},$$

where in euthyroid conditions

$$\text{urine clearance} = 5.8\cdot[I_S],$$

and where the hormonal iodide recycling is based on a simple serum thyroid hormone pool

$$\frac{d}{dt}(\text{hormonal iodide pool}) = \dot{I_H} - 0.32\cdot \text{ hormonal iodide pool},$$

and where

$$\text{hormonal iodide recycling} = 0.25\cdot\text{hormonal iodide pool}.$$

The whole-body iodine metabolism values in [16] were used to parameterize the above equations.

A.6. Thyroid geometry

Our model is concerned with the aggregate behavior of the collection of heterogenous follicles. Since we are interested in the overall input–output behavior, – not that of a singe follicle – the aggregation is simplified by assuming homogenous follicles. A post-mortem study of 1400 normal human thyroid glands [55] indicated the average weight of a thyroid gland was 16.4 g in males ages 20–29, 18.5 g in males ages 30–69, and 14.4 g in females ages 20–69. If the model is given an arbitrary age of 35 years old, a virtual thyroid weight of 18.5 g would be realistic. A separate in-vivo study [56] indicated that thyroid volume was correlated with body weight and age by the following relationship

$$\text{volume} = 1.97 + 0.21\ \text{weight} + 0.06\ \text{age}.$$

This study also indicated that any difference in thyroid size between males and females was due entirely to in body weight. The entire mass of the thyroid, however, is not dedicated to thyroid hormone production. There are also parafollicular cells (cells which secrete calcitonin, an unrelated hormone) present in the thyroid, although much less numerous than standard thyroid follicles [57]. Additionally, there are intrathyroidal capillaries, nerve fibers, and a network of lymphatics contributing to the thyroid volume and weight. Based on a rough inspection of microscopic photographs of thyroid slices in [58], we estimate that about 83% of the thyroid volume is used for thyroid hormone production.

Using a scanning electron microscope, the dimensions of follicular cells in the human thyroid have been measured, with an intermediate diameter of 5-15 μm [59]. A separate study [60] showed that mean follicular diameter was 171 μm. For the purpose of this model, we assume that the normal follicle, cell and colloid, are spherical (see Fig. A.1).

Again, based on estimated from slices in [58] the thyroid follicle volume is assumed to be nominally split between follicular cell and colloid in a 31% to 69% ratio. Scaling for the age and weight relative to a nominal (average) volume is done using the scale factor, *scale*, is simply

$$scale = \frac{1.97 + 0.21 \cdot \text{weight} + 0.06 \cdot \text{age}}{\text{nominal volume}}.$$

A more accurate scaling factor is obtained from measured volume as follows

$$scale = \frac{\text{measured volume} - 0.17 \cdot (1.97 + 0.21 \cdot \text{weight} + 0.06 \cdot \text{age})}{1.97 + 0.21 \cdot \text{weight} + 0.06 \cdot \text{age}}.$$

Thyroid volume changes in response to both TSH and intracellular iodide concentration. A three-dimensional analysis indicates that thyroid cell volume is directly proportional to TSH and inversely proportional to intracellular iodide [61]. Complete absence of TSH caused cells to shrink to 81% of their original volume, and complete absence of iodide causes the cell to grow to 136% of the original volume [61]. These in-vivo effects were produced under chronic TSH stimulation and low iodide for several weeks. We capture this dynamics using a first-order differential equation in terms of the size, termed *size*,

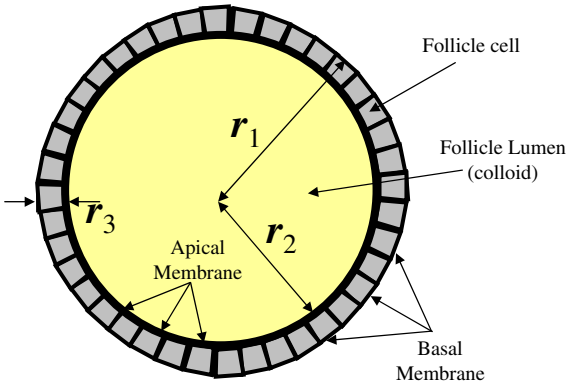

Fig. A.1. Schematic of the thyroid follicle model.

$$\tau_{size}\frac{\mathrm{d}}{\mathrm{d}t}size + size = \mathcal{S}_{cell}^{SSF}\mathcal{I}_{cell}^{I_F}$$

where $\tau_{size} = 504$ (3 weeks) [62] and where $\mathcal{S}_{cell}^{SSF}$ and $\mathcal{I}_{cell}^{I_F}$ are inputs that drive cell size with relation to TSH and follicle cell iodide concentration, respectively. Specifically, these effects are modeled using hyperbolic relations

$$\mathcal{S}_{cell}^{SSF} = 0.81 + \frac{V_{cell}^{SSF}[SSF]}{K_{cell}^{SSF} + [SSF]}, \quad \mathcal{I}_{cell}^{I_F} = \frac{\alpha_{cell}^{I_F}}{K_{cell}^{I_F} + [I_F]},$$

where under nominal physiological conditions, both relation have a numerical value of unity.

As the cell grows with *size*, it becomes columnar extending the basolateral-apical axis dimension [16]. It follows that for a nominal value of 10 μm ([63,64]), the dynamic description of this dimension is

$$\text{follicular cell length} = 10\ size.$$

This follicular cell dimension change is conveniently assumed to be split 25–75% between changes in the basolateral direction and changes in the apical direction, respectively. This simplifying assumption is generally supported in slides shown in [16] for a hypertrophic thyroid. Slides of hypertrophied thyroid follicles that the apical membrane grows convoluted and folded as the follicular cells expand [16]. We further simplify by assuming that the apical surface area remains unchanged as the follicle cells grow.[12] The follicular volume and surface area are determined using simple geometric relations [17].

[12] Slides of hypertrophied thyroid follicles (shown in [16]) indicate that the apical membrane grows convoluted and folded as the follicular cells expand. Its area may actually decrease, but it can no longer be assumed to have any resemblance to a spherical model.

Appendix B. Model parameters

Parameterization of models such as ours in Section 3 is a complicated task especially due to the lack of quantitative data for many variables. Our general process used to identify the parameters is as follows. Initially, we simplify this task by assigning all variables with little known clinical data a nominal value of unity or '1'. We then used the whole body iodine/iodide data in [16] to compute steady-state pools. Next, we relied on a multitude of published clinical and laboratory research to define Michaelis–Menton constants, otherwise we used the standard assumption that many biological processes take place at substrate concentrations close to their Michaelis constant

Table B.1
Model parameters (units if applicable otherwise dimensionless)

$TSH - R = 1$	$K_{NIS}^{SSF} = 8.39$
$K_{turnover}^{NIS} = 129\,600\ \mathrm{h}^{-1}$	$\tau_{decay}^{NIS} = \log 2/120\ \mathrm{m}^2/\mathrm{h}$
$K_{m}^{NIS} = 3300\ \mathrm{nM}$	$V_{rec}^{I_{MD}} = 94\,810\ \mathrm{h}^{-1}$
$K_{rec}^{I_{MD}} = 512\,765\ \mathrm{nM}$	$\tau_{decay}^{I_F} = \log 2/120\ \mathrm{nM}^2$
$A_{bsasl} = 0.5687\ \mathrm{m}^2$	$K_{decay}^{I_F} = 1\ \mathrm{nM}^2$
$\alpha_{apical}^{I_C} = 1 + 7874^3\ \mathrm{nM}^3/\mathrm{m}^2$	$\alpha_{TPO}^{Tg} = 289\ \mathrm{ng/nM/mL}$
$K_{apical}^{I_C} = 7874^3\ \mathrm{nM}^3$	$K_{TPO}^{Tg} = 144.5\ \ \mathrm{ng/mL}$
$V_{1}^{apical} = 306\,740\ \mathrm{h}^{-1}$	$V_{TPO}^{SSF} = 33$
$K_{m1}^{apical} = 33\,000\,000\ \mathrm{nM}$	$K_{TPO}^{SSF} = 32$
$V_{2}^{apical} = 723\ \mathrm{h}^{-1}$	$\alpha_{Tg}^{Tg} = 150\ \ \mathrm{ng/mL/ng/h}$
$K_{m2}^{apical} = 70\,000\ \mathrm{nM}$	$K_{Tg}^{Tg} = 5.5\ \mathrm{mg/mL}$
$V_{apical}^{SSF} = 33$	$V_{Tg}^{SSF} = 33$
$K_{apical}^{SSF} = 32$	$K_{Tg}^{SSF} = 32$
$\tau_{turnover}^{TPO} = 108\,000\ \mathrm{h}^{-1}/\mathrm{mL}$	$V_{Lys}^{SSF} = 69.3$
$V_{org}^{H_2O_2} = 2\ \mathrm{ng/mL}$	$K_{Lys}^{SSF} = 68.3$
$K_{org}^{H_2O_2} = 268\ \mathrm{ng/mL}$	$\alpha_{H_2O_2} = 2175\ \ \mathrm{ng/h}$
$V_{org}^{I_C} = 1\ \mathrm{nM}$	$\tau_{decay}^{H_2O_2} = 1000/267.2^2\ \mathrm{nL}^2/\mathrm{ng}^2/\mathrm{h}$
$K_{org}^{I_C} = 100\,000\ \mathrm{nM}$	$V_{org}^{Tg_{eff}} = 2$
$K_{org}^{Tg_{eff}} = 72\ \mathrm{nM}$	$V_{cell}^{SSF} = 6.19$
$\alpha_{endo} = 0.0112\ \mathrm{mL/m}^2$	$K_{cell}^{SSF} = 31$
$V_{proteo}^{Vac} = 0.0045\ \mathrm{h}^{-1}$	$\alpha_{cell}^{I_F} = 29\,746\ \mathrm{nM}$
$K_{proteo}^{Vac} = 0.0001\ \mathrm{mL}$	$K_{cell}^{I_F} = 21\,874\ \mathrm{nM}$
$V_{NIS}^{SSF} = 7.39$	$A_{apical,nom} = 0.434\ \mathrm{m}^2$
$V_{proteo}^{Lys} = 10$	$A_{basal,nom} = 0.561\ \mathrm{m}^2$
$K_{proteo}^{Lys} = 9$	$V_{follicle,nom} = 5\ \mathrm{mL}$
$\alpha_{NIS}^{I_F} = 3028.5\ \mathrm{nM}$	$V_{colloid,nom} = 11\ \mathrm{mL}$
$K_{NIS}^{I_F} = 10902.5\ \mathrm{nM}$	

[36]. Finally, an iterative process, these were adjusted to achieve reported or expected dynamics under different physiological conditions. The identifies model parameters are presented in Table B.1. Some of these parameters may not reflect actual physical quantities, however, they support our goal of having the resulting model reasonably describe the quantitative nature of relations between inputs and outputs signals.

References

[1] F.A. Mettler, G.L. Voelz, Major radiation exposure what to expect and how to respond, N. Engl. J. Med. 346 (20) (2003) 1554.
[2] L.E. Braverman et al., The effect of perchlorate, thiocyanate, and nitrate on thyroid function in workers exposed to perchlorate long-term, Clin. Endocrinol. Metab. 90 (2) (2005) 700.
[3] Perchlorate (ClO4) and Perchlorate Salts (CASRN 7790-98-9), US EPA, 2005.
[4] D.S. Riggs, Quantitative aspects of iodine metabolism in man, Pharmacol. Rev. 4 (3) (1952) 284.
[5] L.J. Degroot, P. Decostre, R. Phair, A mathematical model of human iodine metabolism, Clin. Endocrinol. Metab. 32 (1971) 757.
[6] M.T. Hays, Kinetics of the human thyroid trap: a compartmental model, Nucl. Med. 19 (1978) 789.
[7] E.A. Merrill et al., PBPK model for radioactive iodide and perchlorate kinetics and perchlorate-induced inhibition of iodide uptake in humans, Toxicol. Sci. 83 (1) (2005) 25.
[8] G. Li, B. Liu, Y. Liu, A dynamical model of the pulsatile secretion of the hypothalomo-pituitary-thyroid axis, Bio Systems 35 (1995) 83.
[9] J.J. Distefano, P.H. Mak, Optimal control policies for the prescription of thyroid hormones, Math. Biosci. 42 (1978) 159.
[10] H. Yamada, J.J. Distefano, Y-M Yen, T.T. Nguyen, Steady-state regulation of whole-body thyroid hormone pool sizes and interconversion rates in hypothyroid and moderately T_3-stimulated rates, Endocrinology 137 (1996) 5624.
[11] J.W. Dietrich, A. Tesche, C.R. Pickardt, U. Mitzdorf, Fractal properties of the thyrotropic feedback control implications of a nonlinear model compared with empirical data, Proc. Cybern. Syst. Conf. (2002) 329.
[12] J.J. DiStefano, A model of the normal thyroid hormone glandular secretion mechanism, J. Theor. Biol. 22 (1969) 412.
[13] M. Eisenberg, M. Samuels, J.J. DiStefano, L$-T_4$ bioequivalnce and hormone replacement studies via feedback control simulations, Thyroid 16 (2007) 1279.
[14] V. Misra, W. Gong, D. Towsley, A fluid-based analysis of a network of AQM routers supporting TCP flows with an application to RED, Proc. ACM SIGCOMM, Stockholm, Sweden, 2000.
[15] P. Indelman, Averaging of unsteady flows in heterogeneous media of stationary conductivity, J. Fluid Mech. 310 (1996) 39.
[16] F.S. Greenspan, D.G. Gardner, Basic & Clin. Endocrinol., seventh ed., McGraw-Hill, New York, 2004.
[17] M.S. Degon, A Quantitative Model of the Human Thyroid: Development, Analysis, and Observations, M.S. Thesis, University of Massachusetts, Amherst, 2005.
[18] M.S. Degon, Y. Chait, C.V. Hollot, S. Chipkin, T. Zoeller, A quantitative model of the human thyroid: development and observations, Proc. Am. Control Conf., Portland, OR, 2005.
[19] O. Dohn et al., The sodium/iodide symporter (NIS): characterization, regulation, and medical significance, Endocr. Rev. (2003) 24.
[20] B. Rapoport, The thyrotropin receptor, in: L.E. Braverman, R.D. Utiger (Eds.), Werner & Ingbar's the Thyroid: A Fundamental and Clinical Text, Lippincott Williams and Wirlkins, NY, 2000, p. 219.
[21] T. Kogai et al., Regulation by thyroid-stimulating hormone of sodium iodide symporter gene expression and protein levels in frtl-5 cells, Endocrinology 138 (1997) 2227.
[22] A.M. Taurog, Hormone synthesis: thyroid iodine metabolism, in: L.E. Braverman, R.D. Utiger (Eds.), Werner & Ingbar's the Thyroid: A Fundamental and Clinical Text, Lippincott Williams and Wirlkins, NY, 2000, p. 61.

[23] J.T. Dunn, A.D. Dunn, Thyroglobulin, in: L.E. Braverman, R.D. Utiger (Eds.), Werner & Ingbar's the Thyroid: A Fundamental and Clinical Text, Lippincott Williams and Wirlkins, NY, 2000, p. 91.
[24] F. Bogazzi et al., Thyroid color flow doppler sonography: an adjunctive tool for differentiating patients with inappropriate thyrotropin (TSH), secretion due to TSH-secreting pituitary adenoma or resistance to thyroid hormone, Thyroid 16 (10) (2006) 989.
[25] P.H.K. Eng et al., Escape from the acute Wolff–Chaikoff effect is assosciated with a decrease in thyroid sodium/iodide smporter messenger ribonucleic acid and protein, Endocrinology 140 (1999) 3404.
[26] P.H.K. Eng et al., Regulation of the sodium iodide symporter by iodide in FRTL-5 cells, Eur. J. Endocrinol. 144 (2001) 139.
[27] K. Suzuki et al., Autoregulation of thyroid-specific gene transcription by thyroglobulin, PNAS 95 (1998) 8251.
[28] R.C. Marians, L. Ng, H.C. Blair, P. Unger, T.F. Davies, Defining thyrotropin-dependent and -independent steps of thyroid hormone synthesis by using thyrotropin receptor-null mice, PNAS 99 (2002) 15776.
[29] MATLAB and Simulink, The MathWorks, Natick, MA, 2007.
[30] K.L. Caldwell, R. Jones, J.G. Hollowell, Urinary iodine concentration: United States national health and nutrition examination survey 2001–2002, Thyroid 15 (7) (2005) 692.
[31] R.C. Dorf, R.H. Bishop, Modern Control Systems, tenth ed., Prentice Hall, NJ, 2005.
[32] S. Greenspan, A. Klibanski, D. Schoenfeld, E.C. Ridgeway, Pulsitile secretion of thyrotropin in man, Clinical Endocrinology & Metabolism 63 (1986) 661.
[33] G. Riesco-Eizaguirr, P. Santisteban, A perspective view of sodium iodide symporter research and its clinical implications, Eur. J. Endocrinol. 155 (2006) 495.
[34] C. Spitzweg, W. Joba, J.C. Morris, A.E. Heufelder, Regulation of sodium iodide symporter gene expression in FRTL-5 rat thyroid cells, Thyroid 9 (1999) 821.
[35] C.F. Andrea et al., Rapid regulation of thyroid sodiumiodide symporter activity by thyrotrophin and iodine, Endocrinology 184 (2005) 69.
[36] G.A. Truskey, F. Yuan, D.F. Katz, Transport Phenomena in Biological Systems, Pearson Prentice Hall, NJ, 2004.
[37] J.G. Wagner, G.J. Szpunar, J.J. Ferry, A nonlinear physiologic pharmacokinetic model: I. Steady-state, Pharmacokinet. Pharmacodyn. 13 (1) (1985) 73.
[38] E.M. Brown, Four-parameter model of the sigmoidal relationship between parathyroid hormone release and extracellular calcium concentration in normal and abnormal parathyroid tissue, Clin. Endocrinol. Metab. 56 (1983) 572.
[39] F.M. Delange, J.T. Dunn, Iodine deficiency, in: L.E. Braverman, R.D. Utiger (Eds.), Werner & Ingbar's the Thyroid: A Fundamental and Clinical Text, Lippincott Williams and Wirlkins, NY, 2000, p. 264.
[40] J. Van Sande, S. Sillens, J.E. Dumont, Adenosine 3′,5′-monophosphate metabolism and turnover in dog thyroid slices, Eur. J. Biochem. 72 (1977) 241.
[41] S. Eskandari et al., Thyroid Na^+/I^- symporter: mechanism, stoichiometry, and specificity, Biol. Chem. 272 (1997) 27230.
[42] N. Carrasco, Thyroid iodide transport: the Na^+/I^- Symporter (NIS), in: L.E. Braverman, R.D. Utiger (Eds.), Werner & Ingbar's the Thyroid: A Fundamental and Clinical Text, Lippincott Williams and Wirlkins, NY, 2000, p. 52.
[43] S. Gnidehou et al., Iodotyrosine dehalogenase 1 (DEHAL1) is a transmembrane protein involved in the recycling of iodide close to the thyroglobulin iodination site, FASEB J. 18 (13) (2004) 1574.
[44] A.C. Bianco, P.R. Larsen, Intracellular pathways of iodothyronine metabolism, in: L.E. Braverman, R.D. Utiger (Eds.), Werner & Ingbar's the Thyroid: A Fundamental and Clinical Text, Lippincott Williams and Wirlkins, NY, 2000, p. 109.
[45] D.H. Solomon, J.T. Dowling, The thryoid, Annual Reviews Physiology 22 (1960) 615.
[46] W.L. Green, Effects of 3-nitro-L-tyrosine on thyroid function in the rat: an experimental model for the dehalogenase defect, Clin. Invest. 50 (1971) 2474.
[47] A.M. Rodriguez et al., Identification and characterization of a putative human iodide transporter located at the apical membrane of thyrocyctes, Clin. Endocrinol. Metab. 87 (2002) 3500.
[48] D.A. Scott et al., The pendred syndrome gene encodes a chloride–iodide transport protein, Natl. Genet. 21 (1999) 440.

[49] P. Golstein, M. Abramow, J.E. Dumont, R. Beauwens, The iodide channel of the thyroid: a plasma membrane vesicle study, Cell Physiol. 263 (1992) C590.
[50] M.P. Gillam, A.R. Sidhaye, E.J. Lee, J. Rutishauser, C.W. Stephan, P. Kopp, Functional characterization of pendrin in a polarized cell system: evidence for pendrin-mediated apical iodide efflux, Biol. Chem. 279 (13) (2004) 13004.
[51] P. Kopp, Thyroid Hormone Synthesis, in: L.E. Braverman, R.D. Utiger (Eds.), Werner & Ingbar's the Thyroid: A Fundamental and Clinical Text, Lippincott Williams and Wirlkins, NY, 2000, p. 52.
[52] M.A. Pisarev, R. Gärtner, Autoregulatory Actions of Iodine, in: L.E. Braverman, R.D. Utiger (Eds.), Werner & Ingbar's the Thyroid: A Fundamental and Clinical Text, Lippincott Williams and Wirlkins, NY, 2000, p. 85.
[53] A. Haeberli, H. EnglerH, C. Grunigen, H. Kohler, H. Studer, Low molecular weight intracellular iodocompounds with long intrathyroidal half-life: remnants of thyroglobulin hydrolysis, Acta Endocrinol. 92 (1) (1979) 105.
[54] R. Ekholm, U. Björkman, Glutathione peroxidase degrades intracellular hydrogen peroxide and thereby inhibits intracellular protein iodination in thyroid epithelium, Endocrinology 138 (7) (1997) 2871.
[55] B.G. Pankow, J. Michalak, M.K. McGee, Adult human thyroid weight, Health Phys. 49 (1985) 1097.
[56] L. Hegedus et al., The determination of thyroid volume by ultrasound and its relationship to body weight, age, and sex in normal subjects, Clin. Endocrinol. Metab. 56 (1983) 260.
[57] C.C. Capen, Comparative anatomy and physiology, in: L.E. Braverman, R.D. Utiger (Eds.), Werner & Ingbar's the Thyroid: A Fundamental and Clinical Text, eighth ed., Lippincott Williams and Wirlkins, NY, 2000, p. 20.
[58] R.A. Bergman, A.K. Afifi, P.M. Heidger, Atlas of Microscopic Anatomy, Section 15 – Endocrine Glands, WB Saunders Co., Canada, 1989.
[59] M. Sobrinho, J.V. Johannessen, Scanning electron microscopy of the normal human thyroid, Submicrosc. Cytol. 13 (1981) 209.
[60] A. Faggiano, Age-dependent variation of follicular size and expression of iodine transporters in human thyroid tissue, Nucl. Med. 45 (2004) 232.
[61] D. Cauvi et al., Regulation of thyroid cell volumes and fluid transport, Endocrinol. Metab. 279 (2000) E546.
[62] E. Namba et al., Evidence of thyroid volume increase in normal subjects receiving excess iodide, Clin. Endocrinol. Metab. 76 (1993) 605.
[63] A. Faggiano, Age-dependent variation of follicular size and expression of iodine transporters in human thyroid tissue, Nucl. Med. 45 (2) (2004) 232.
[64] M. Sobrinho, J.V. Johannessen, Scanning electron microscopy of the normal human thyroid, Submicrosc. Cytol. 13 (2) (1981) 209.